

# ELECTRICAL EROSION RESISTANCE OF GRAPHENE REINFORCED CU-W CIRCUIT BREAKER CONTACT MATERIALS UNDER 5 KA ARC

X. WANG<sup>a</sup>, Y.N. ZHOU<sup>b</sup>, A. CONNOLLY<sup>c</sup>, S.Y. MATHARAGE<sup>a</sup>, M. BISSETT<sup>c</sup>,  
J.W. SPENCER<sup>b</sup>, J.D. YAN<sup>b</sup>, I. KINLOCH<sup>c</sup>, Z.D. WANG<sup>a,\*</sup>

<sup>a</sup> Centre for Smart Grid, Department of Engineering, University of Exeter. EX4 4PY, UK

<sup>b</sup> Department of Electrical Engineering and Electronics, University of Liverpool, Liverpool L69 3GJ, UK

<sup>c</sup> Department of Materials, University of Manchester, Manchester M13 9PL, UK

\* zhongdong.wang@exeter.ac.uk

**Abstract.** This work integrates experimental and MD simulation approaches to study the role of graphene in G-Cu-W composites. Arcing tests were conducted on G-Cu-W and Cu-W contact samples under a 5 kA peak current. Experimental results show that adding graphene leads to a lower surface roughness of the sample following arcing. MD simulation results indicate that the G-Cu-W model exhibits a smoother surface and fewer lost metal atoms than the Cu-W model due to the protective effect of graphene layer.

**Keywords:** Circuit breaker contact, Graphene-reinforced Cu-W composites, Arc erosion, Molecular dynamics simulation.

## 1. Introduction

Copper-tungsten (Cu-W) contacts have gathered considerable experience over decades for their use in high-voltage circuit breakers (HVCBs). These contacts combine the high electrical conductivity of Cu with the high mechanical strength, high melting point, and low thermal expansion of W. During faulty conditions when the current exceeds tens of thousands of Amps, the opening of a circuit breaker results in a highly destructive arc. Although Cu-W contacts are capable of withstanding repeated arcing processes during operation, their limited operating lifetime remains a challenge due to the erosive effects of arcing conditions that damage the contact surface, leading to compromised structural integrity and electrical performance.

Graphene is a 2D nanomaterial composed of a monoatomic layer of hexagonally arranged carbon atoms known for their exceptional mechanical, thermal, and electrical properties. Recent studies have focused on the incorporation of graphene as an additive to enhance the properties of Cu-W contact materials. Study [1] indicated that the addition of graphene can improve the hardness and conductivity of the Cu-W matrix. Study [2] reported that adding graphene can enhance the breakdown strength of W70Cu30 composites. However, these results are only based on the small bulk samples, and the experimental environment is far from the practical circuit breaker's working conditions. Therefore, it is still unclear if graphene can improve the lifetime of circuit breaker contacts and what the anti-erosion mechanism of graphene is.

This work studies the failure mechanism of circuit breaker contacts and the role of graphene in G-Cu-W composites by implementing arcing tests on Cu-W (80 wt% W and 20 wt% Cu) and G-Cu-W (80 wt% W,

20 wt% Cu and 0.02 wt% G) circuit breaker contacts under 5 kA peak current condition. In addition, Molecular Dynamics (MD) simulation is used to study the electrical erosion resistance mechanism of graphene at the micro-level.

## 2. Experiment Setup

The testing HVCB unit is a modification of a 245 kV/40 kA live tank circuit breaker. The schematic diagram of the HVCB unit without the nozzle is shown in Figure 1, which gives the relative positions of arcing contacts. In Figure 1(b), the main circuit of the experimental system is composed of a charging circuit, a capacitor bank, a dump circuit, a test current trigger circuit and a test circuit breaker. The capacitor bank is used as the power source of the arcing current. There are four ignitrons to turn current on or off in the main circuit: the dump ignitron, DC ignitron, forward and reverse AC ignitrons. An ignitron is a gas-filled tube used to control the current in a circuit.

The arc voltage and current are measured using a high-voltage probe (Tektronix P6015 A) and a Rogowski coil respectively, and the data is recorded by a digital oscilloscope (Tektronix DPO 2024). The typical waveforms (arc voltage and current) are shown in Figure 2. Before the arcing contacts are separated, a low and slowly decaying DC current passes through the arcing contacts and maintains an arc for tens of milliseconds. At a certain point in time after contact separation, a positive half-cycle AC is then generated, and the arc is extinguished automatically at the first current zero crossing point. The present work conducted one time 5 kA current peak sine half-wave arcing test on the G-Cu-W and Cu-W contacts, respectively.

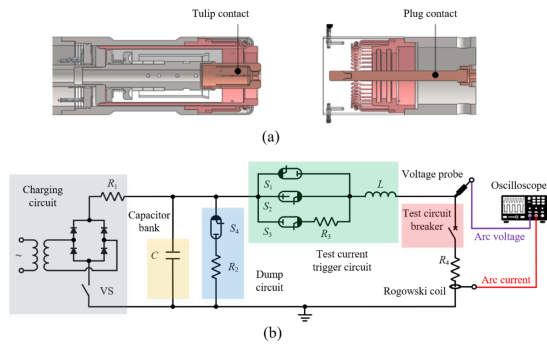


Figure 1. (a) Schematic diagram of the HVCB without nozzle; (b) schematic diagram of the main circuit.

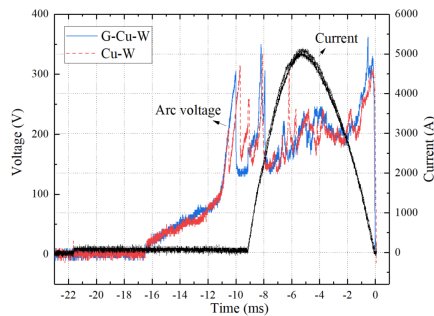


Figure 2. Current and voltage waveforms under 5 kA arcing condition.

### 3. Material Characterisation

Raman spectroscopy and Raman mapping are employed to determine the distribution of graphene across the surface of the G-Cu-W contact samples using a Renishaw inVia Qontor confocal Raman microscope, under illumination of a 532 nm laser. Spectral acquisition was performed on different locations on the surface of the contact head. In Figure 3(b), a Raman intensity map can be seen, which shows the intensity of the characteristic G-peak Raman signal associated with graphene on the G-Cu-W contact surface. The graphene signal is located predominantly in the Cu-rich regions, indicating that some graphene fillers are distributed across the Cu phase of the G-Cu-W composite.

The Scanning Electron Microscope (SEM) image of the Cu-W contact surface of the cathode subjected to a single arcing test is shown in Figure 4(a). Cu (black phase) and W (white phase) can still be observed. However, the W grain structures are no longer visible. Instead, some melting and resolidification of the W skeleton can be observed. Figure 4(b) shows the SEM image of the G-Cu-W contact surface subjected to a single arcing test. W grains can still be observed on the contact surface, with interstitial Cu domains remaining. Arc erosion has not entirely eroded the surface Cu, indicating contacts can maintain a low resistance state in the closed position. This represents a significant difference in performance from Cu-W contacts. The presence of graphene provides reinforcement of the Cu-W metal matrix, as well as absorbing

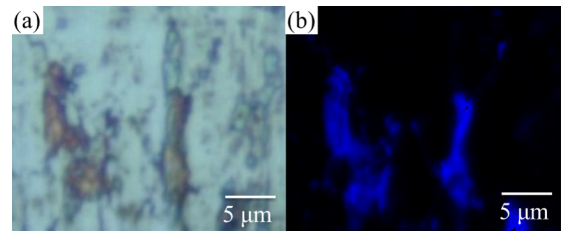


Figure 3. (a) White-light image of G-Cu-W contact surface before arcing test, showing Cu-heavy region. (b) Raman intensity map of graphene G-peak ( $1580\text{ cm}^{-1}$ ) of the same region. The G-peak signal is coloured blue – the brighter the blue in the image indicates a stronger G-peak signal.

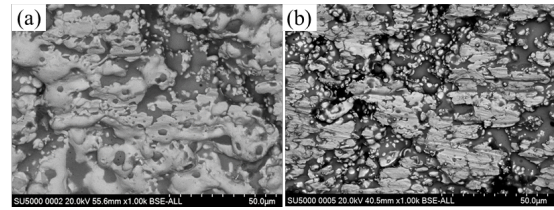


Figure 4. SEM images of cathode contact surface after a single arc shot at 5 kA of (a) Cu-W; (b) G-Cu-W.

energy during the arcing process, reducing damage to the contact surface.

Laser scanning confocal microscopy is utilised to establish roughness parameters of the contact surface after the arcing test. As shown in Figure 5, the surface roughness, which measures the average deviation of a surface profile from a flat plane, increases after the arcing test compared with the contact surface before the arcing test. Across this range, the G-Cu-W contacts exhibit a lower surface roughness than the Cu-W contacts.

## 4. Anti-erosion Mechanism of Graphene at Micro-level

### 4.1. Simulation Details

The Cu-W model, depicted in Figure 6(a), represents a typical Cu-W composite structure where Cu fills the gaps between W grains. Based on the Raman mapping results, graphene is found in the Cu-rich region of the contact surface. To incorporate this, a single layer of graphene is added to the Cu surface of the Cu-W model, forming a G-Cu-W model shown in Figure 6(b). The fixed boundary condition is used along the z direction, while the periodical boundary condition is applied in the x and y directions. Additionally, three bottom layers of substrates are fixed. Both models are first energy minimised and then fully relaxed at 300 K for 30 ps before ion bombardment simulation. Then, three models' atom layers at all four vertical surfaces are forced to maintain 300 K to prevent the waves caused by the bombardment from returning through the periodic boundary. It is noted that neutral sulphur (S) atoms instead of S ions are

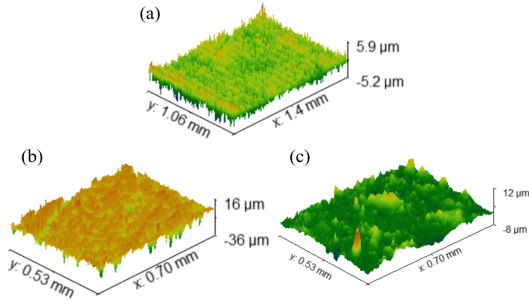


Figure 5. 3D confocal microscopy profile scans of (a) contact surface before arcing; (b) Cu-W and (c) G-Cu-W composite contact surfaces after arcing.

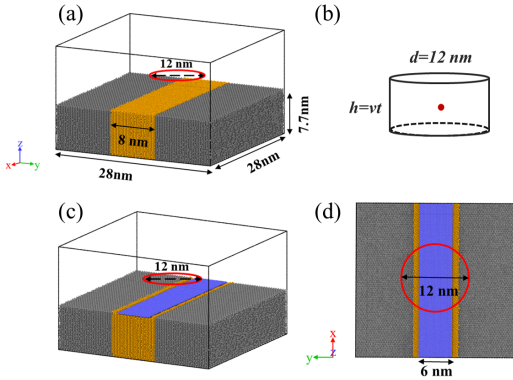


Figure 6. (a) Cu-W model, (b) the space independently occupied by each incident ion, (c) G-Cu-W model with the same dimensions of Cu-W model, (d) Top view of G-Cu-W. Red circle shows the position of incident area. Black, yellow and blue particles represent W, Cu and C atoms

used to bombard the models in the simulation, as ions are neutralised before bombarding the surface in the practical working environment [3].

Due to the complexity of arc erosion process, only the impact of ion bombardment is studied as one of the critical erosion processes in this work. In the simulation, the model surface is one-by-one bombarded by 1500 S ions from random sites within a circular region with a diameter of 12 nm above the model surface. The energy of each incident ion is 50 eV, which combines thermal energy from the arc, kinetic energy from the voltage drop and recombination energy [3]. The time interval between continuous incident atoms is set as 0.1 ps. Figure 6(b) exhibits the space independently occupied by each incident ion. Therefore, the particle density (average number of particles in unit volume) of S ions in the simulation is  $5.10 \times 10^{18} \text{ cm}^{-3}$ , which is consistent with the particle density ( $10^{17}$  to  $10^{18} \text{ cm}^{-3}$ ) in [4]. An NVE (constant Number of particles, Volume, and Energy) ensemble is used during the ion bombardment process, with a variable timestep depending on the incident energy. After the bombardment of 1500 ions, models are cooled down to 300 K.

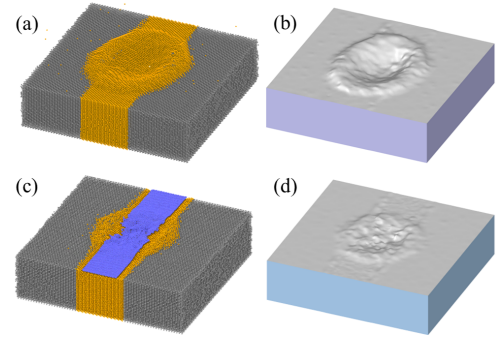


Figure 7. Surface morphologies of models after ion bombardment and cooling down to 300 K: (a) and (b): Cu-W; (c) and (d): G-Cu-W.

Classic MD simulations are performed using the Large-scale Atomic/Molecular Massively Parallel Simulator (LAMMPS). The adaptive intermolecular reactive empirical bond order (AIREBO) potential describes the interactions between C atoms in graphene. The embedded-atom method (EAM) is used to describe the interactions between Cu atoms and W atoms. The interactions of the Cu-C atom pairs and W-C atom pairs are described by 12-6 Lennard-Jones (LJ) potentials [5, 6]. The interactions between the incident S atom with C, Cu, W and other S atoms are calculated with the Ziegler-Biersack-Littmark (ZBL) repulsive potential [7].

## 4.2. Simulation Results

Surface morphologies of Cu-W and G-Cu-W models after ion bombardment and cooling down to 300 K are shown in Figure 7. In the Cu-W system, a large erosion crater is formed on the surface, as shown in Figure 7(a) and the corresponding surface mesh Figure 7(b). This phenomenon is attributed to the movement of metal atoms away from the incident region under ion bombardment, leading to some atoms being sputtered from the surface. Simultaneously, metal atoms gain energy through collisions, causing Cu with a low melting point to rapidly melt and expand, eventually overflowing from the gaps between W grains and forming an erosion crater on the surface. However, no distinct erosion crater is formed on the G-Cu-W surface, as shown in Figure 7(c) and (d). In comparison to the Cu-W system, the G-Cu-W system demonstrates a noticeable reduction in the number of Cu atoms overflowing from the gaps between W grains. This reduction contributes to a relatively smoother surface in the G-Cu-W system, consistent with the results obtained from confocal microscopy.

Table 1 compares the number of lost metal atoms between the Cu-W and G-Cu-W systems, revealing a significantly lower number of lost metal atoms in the G-Cu-W system. This reduction can be attributed to graphene with exceptional strength and a high melting point. The graphene layer on the surface acts as a barrier, preventing direct ion bombardment on the

Contact material	Number of lost atoms
Cu-W	785 Cu atoms
G-Cu-W	136 Cu atoms, 99 C atoms

Table 1. Number of lost metal atoms

model surface. The majority of the incident energy is absorbed by the graphene layer and dissipated in the form of waves to the surroundings, thereby reducing the energy exerted on the metal atoms. Additionally, the graphene layer prevents the underlying Cu atoms from leaving the surface, thereby enhancing the resistance to arc erosion in the Cu-W composites. It is worth noting that in both systems, the lost metal atoms are exclusively Cu atoms, indicating that W exhibits better resistance to arc erosion than Cu due to its higher melting point and strength. In addition simulation results revealed that the edges of graphene are more susceptible to damage because the carbon atoms at the edges indeed lack C-C bonds compared to the internal C atoms, resulting in reduced strength.

Figures 8(a) and (b) show cross-sectional images of the Cu-W and G-Cu-W systems after ion bombardment, respectively. The surface expansion observed in the Cu-W model is higher than that in the G-Cu-W model. Figures 8(c) and (d) display the corresponding atomic temperature distributions, where the temperature of part atoms exceeds the melting point of Cu (1357 K) and W (3695 K). It can be seen that the hottest region (3700 K) in Cu-W model is significantly larger than that in the G-Cu-W model. This is attributed to the much lower thermal conductivity across the G/Cu interface than the Cu matrix. Consequently, the heat in graphene cannot rapidly conduct to the underlying Cu matrix. Figures 8(e) and (f) show the morphologies of W grains on the right side of both models, indicating greater damage to W grains in the Cu-W system than in the G-Cu-W system, which agrees with SEM results.

## 5. Conclusions

In this work, experimental and MD simulation were integrated to study the role of graphene in G-Cu-W contact materials. Arcing tests were conducted on G-Cu-W and Cu-W contact samples under a 5 kA peak current. Experimental findings revealed that the addition of graphene reduced the damage to contact surface and surface roughness of the Cu-W matrix following arcing tests. MD simulations demonstrated that the graphene-covered Cu-W model exhibited a smoother surface and fewer lost metal atoms compared to the Cu-W model, which agrees with the material characterisation results. This can be attributed to graphene acting as a protective layer, effectively reducing the incident energy on the substrate. In addition, graphene prevents heat transfer to the substrate, significantly reducing the molten pool's size.

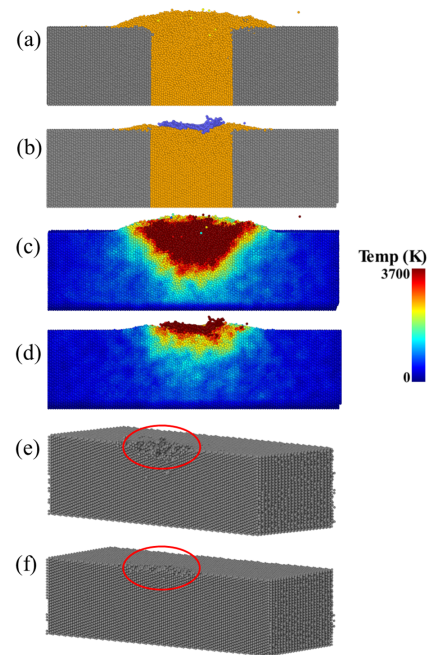


Figure 8. Cross section of (a) Cu-W and (b) G-Cu-W after ions bombardment; (c) and (d) are corresponding temperature distribution profiles. (e) and (f) are W bulk on right side after cooling to 300 K.

## Acknowledgements

This work was supported by the State Grid Corporation of China Science and Technology Foundation (5500-201958505A-0-0-00).

## References

- [1] L. Dong, W. Chen, C. Zheng, and N. Deng. Microstructure and properties characterization of tungsten-copper composite materials doped with graphene. *Journal of Alloys and Compounds*, 695:1637–1646, 2017. doi:10.1016/j.jallcom.2016.10.310.
- [2] L. Dong, W. Chen, N. Deng, et al. Investigation on arc erosion behaviors and mechanism of W70Cu30 electrical contact materials adding graphene. *Journal of Alloys and Compounds*, 696:923–930, 2017. doi:10.1016/j.jallcom.2016.12.044.
- [3] R. Xu, M. Zhou, X. Wang, et al. A molecular dynamics simulation study on the role of graphene in enhancing the arc erosion resistance of Cu metal matrix. *Computational Materials Science*, 212:111549, 2022. doi:10.1016/J.COMMATSCI.2022.111549.
- [4] H. Ito et al. *Switching Equipment*. Springer, 2019. doi:10.1007/978-3-319-72538-3.
- [5] W. Peng and K. Sun. Effects of Cu/graphene interface on the mechanical properties of multilayer Cu/graphene composites. *Mechanics of Materials*, 141:103270, 2020. doi:10.1016/J.MECHMAT.2019.103270.
- [6] A. Dinsdale. Sgte data for pure substances. *Calphad*, 15(4):317–425, 1991. doi:10.1016/0364-5916(91)90030-N.
- [7] J. F. Ziegler and J. P. Biersack. *The stopping and range of ions in matter*. Springer, 1985. doi:10.1007/978-1-4615-8103-1\_3.